MMC-Based SRM Drives With Decentralized Battery Energy Storage System for Hybrid Electric Vehicles

Chun Gan, *Member, IEEE*, Qingguo Sun, Jianhua Wu, Wubin Kong, *Member, IEEE*, Cenwei Shi, and Yihua Hu, *Senior Member, IEEE*

***Abstract*—This paper proposes a modular multilevel converter (MMC) based switched reluctance motor (SRM) drive with decentralized battery energy storage system for hybrid electric vehicle applications. In the proposed drive, a battery cell and a half-bridge converter is connected as a submodule (SM), and multiple SMs are connected together for the MMC. The modular full-bridge converter is employed to drive the motor. Flexible charging and discharging functions for each SM are obtained by controlling switches in SMs. Multiple working modes and functions are achieved. Compared to conventional and existing SRM drives, there are several advantages for the proposed topology. A lower dc-bus voltage can be flexibly achieved by selecting SM operation states, which can dramatically reduce the voltage stress on the switches. Multilevel phase voltage is obtained to improve the torque capability. Battery state-of-charge balance can be achieved by independently controlling each SM. Flexible fault-tolerance ability for battery cells is equipped. The battery can be flexibly charged under both running and standstill conditions. Furthermore, a completely modular structure is achieved by using standard half-bridge modules, which is beneficial for market mass production. Experiments carried out on a three-phase 12/8 SRM confirm the effectiveness of the proposed SRM drive.**

***Index Terms*—Battery fault tolerance, charging and discharging, flexible dc-bus voltage, hybrid electric vehicle (HEV), modular multilevel converter (MMC), switched reluctance motor (SRM).**

I. Introduction

With clean energy requirements in urban transportations, electric vehicles (EVs) and hybrid EVs (HEVs) have received much attention owing to their fuel-efficient performance and protection of the environment against exhaust emission, which have been significantly supported all over the world [1]–[5]. However, considering the driving range anxiety issue and control flexibility, HEVs have been a compromise solution

Manuscript received January 31, 2018; revised April 25, 2018; accepted May 31, 2018. Date of publication June 11, 2018; date of current version February 5, 2019. Recommended for publication by Associate Editor B. Fahimi. *(Corresponding author: Wubin Kong.)*

C. Gan and W. Kong are with the State Key Laboratory of Advanced Electromagnetic Engineering and Technology, School of Electrical and Electronic Engineering, Huazhong University of Science and Technology, Wuhan 430074, China (e-mail:

for three-phase motors. In [27], an improved C-dump converter is presented with integrated charging capability. However, the converter topology has poor fault-tolerance ability due to reduced switches and the multilevel phase voltage is not achieved. In [28], a tri-port drive is put forward to achieve integrated grid-connected charging ability. But the dc-bus voltage cannot be flexibly changed and three phases share one switch leading to poor fault-tolerance ability. Multiport converter topologies are proposed in [29] and [30] for HEVs to improve the torque performance and to achieve battery charging. However, modular structure, flexible dc-bus voltage, and battery fault tolerance are not achieved. In [31], modular power modules are employed to form a modified Miller converter, while fault-tolerance ability for each phase and batteries are not achieved.

Considering that the required dc-bus voltage in low-speed operations is much lower than that in high-speed operations, the voltage stress on the switches and the switching loss can be reduced in the inverter/converter with a lower dc-bus voltage [32]. Furthermore, the reliability of the switches can be enhanced due to a much lower voltage stress [33]. Considering this point, an SRM converter with a dc-link chopper is proposed in [34], where the dc-bus voltage is controlled by the chopper as a function of the motor speed. However, an additional inductor and capacitor need to be used and multilevel phase voltage is not achieved. Also, this converter is derived from a split dc-link four-switch converter without phase isolation, leading to poor fault-tolerance ability and control flexibility. SRM drives with a front-end dc–dc converter are presented in [35] and [36] to obtain variable dc-bus voltage and battery charging ability, while the additional use of inductors and capacitors reduces the power density, and the modular structure and flexible battery fault-tolerance ability are not achieved.

Due to the highly modular structure, multilevel voltage, and inherently bidirectional characteristic, modular multilevel converters (MMCs) have been employed for ac machines to improve sinusoidal waveforms for system performance enhancements [37]–[40]. Multilevel converter topologies have been investigated for SRMs to enhance the torque capability, improve the high-speed performance, and reduce the power loss for high-speed and high-power applications [20], [41]. Considering that the MMC can provide not only the multilevel voltage, but also the modular structure, flexible output voltage, and independent submodule (SM) control, it can be explored for SRM drives to improve the whole system performance and achieve integrated multiple functions. Therefore, this paper takes advantages of the MMC topology for SRM drives to achieve multilevel phase voltage, flexible dc-bus voltage, modular structure, and flexible SM control. By developing the MMC topology for SRM drives, the torque can be improved due to the multilevel voltage, the voltage stress on the switches can be reduced with flexible dc-bus voltage. Furthermore, the flexible battery fault-tolerance ability, and flexible discharging and charging functions can be achieved due to the independent SM control.

In the proposed MMC-based SRM drive, multiple working modes are achieved, including the battery driving mode, generator control unit (GCU) driving mode, GCU-battery driving mode, running charging mode, standstill charging mode, and battery fault-tolerance mode. The advantages of the proposed topology are as follows.

1) Multiple working modes can be flexibly selected by controlling the MMC and full-bridge converter.
2) The MMC-based topology can drive the SRM from variable dc voltages according to the running speed to reduce the voltage stress on the switches which also improves the reliability.
3) Multilevel phase voltage is achieved due to additional battery charging under running conditions, which improves the torque capability.
4) By using standard half-bridge modules for both the MMC and full-bridge converter, completely modular topology is achieved.
5) Flexible charging functions can be directly achieved through the proposed drive without external ones, including the running charging and standstill charging modes.
6) Flexible fault-tolerance ability for each battery cell is equipped by easily bypassing the faulty one.
7) The battery state-of-charge (SOC) can be balanced by controlling the SM charging according to the SOC level.

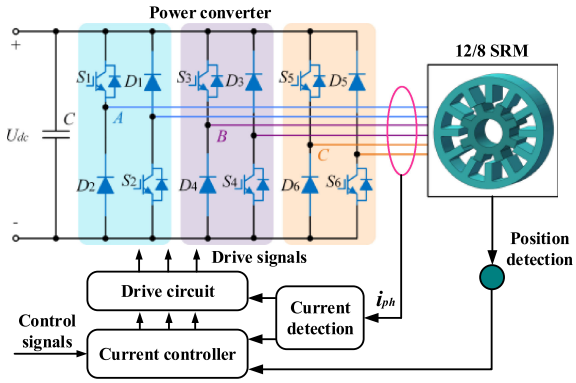

Fig. 1. Diagram of the three-phase 12/8 SRM drive.

This paper is organized as follows. Section II presents the conventional SRM drive. Section III proposes a new MMC-based SRM drive for HEV applications; the driving mode, charging mode, variable dc-bus voltage, and battery fault-tolerance mode are investigated; the current flow and phase voltage are analyzed; a detailed comparison of the proposed and existing topologies is presented. The proposed drive topology is verified by experiments in Section IV. Finally, the conclusion is given in Section V.

II. Conventional SRM Drives

Fig. 1 illustrates the diagram of a three-phase 12/8 SRM drive, mainly including a power converter, an SRM, a drive circuit, current sensors, a position sensor, and a current controller. Phase currents are detected by individual current sensors for the implementation of the current control strategy. Considering the phase-isolation characteristic and excellent fault-tolerance capability, the asymmetrical half-bridge converter is usually employed for the SRM drive, where each phase leg can be independently controlled by two switching devices. For the current controller, the hysteresis control method is usually used. The

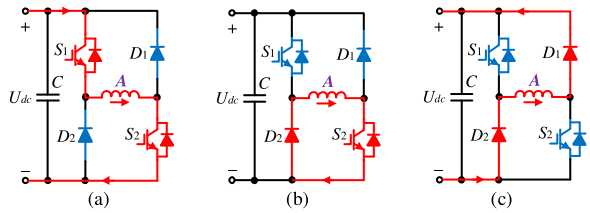

Fig. 2. Switching modes of the asymmetrical half-bridge converter. (a) Excitation mode. (b) ZVL mode. (c) Demagnetization mode.

hysteresis control system is a nonlinear system, which has excellent loop performance, global stability, and small phase lag. Therefore, the current hysteresis control is inherently stable and robust to dynamic perturbations, and the system is more stable and has fast dynamic response due to its inherent nonlinearity.

Fig. 2 shows the three switching modes of phase A in the asymmetrical half-bridge converter, including the excitation mode, freewheeling mode, and demagnetization mode. When switches S_1 and S_2 are both turned ON, the dc power source supplies the current to the phase A winding, and this phase works in the excitation mode [see Fig. 2(a)] where the phase voltage is positive dc-bus voltage $U_{\rm dc}$; when switch S_1 is turned OFF and S_2 is still ON, the phase A current flows through S_2 and diode D_2 in a zero-voltage loop (ZVL), where phase A is in the ZVL mode [see Fig. 2(b)]. When switches S_1 and S_2 are both turned OFF, the phase A current flows back to the dc source through diodes D_1 and D_2, and phase A is in the demagnetization mode [see Fig. 2(c)], where the phase voltage is negative dc-bus voltage $-U_{\rm dc}$.

The voltage equation for each phase can be expressed in terms of the current, inductance, and rotor position as

$$U_k = R_k i_k + L_k(\theta, i_k)\frac{di_k}{dt} + \frac{\partial L_k(\theta, i_k)}{\partial \theta}\omega i_k \qquad (1)$$

where U_k is the phase voltage, R_k is the phase winding resistance, i_k is the phase current, θ is the rotor position, L_k is the phase winding inductance that varies as a function of the rotor position, ω is the rotor angular speed, and $k = a, b, c$ phases.

The output torque of the three-phase SRM is the sum of individual phase torques, which is expressed as

$$T_e = \sum_{k=1}^{3} T_{ek} = \sum_{k=1}^{3} \frac{1}{2} {i_k}^2 \frac{\partial L_k(i_k, \theta)}{d\theta}. \qquad (2)$$

When a current is applied in the inductance ascending region, a positive phase torque can be obtained, while applying a current to a phase winding in the inductance descending region leads to a negative phase torque.

The mechanical equation of the SRM is expressed as

$$J\frac{d\omega}{dt} + \mu\omega = T_e - T_l \qquad (3)$$

where T_e is the output torque, T_l is the load torque, J is the combined moment of inertia of the motor and load, and μ is the combined friction coefficient of the motor and load.

However, for conventional SRM drives, the dc-bus voltage is fixed and the voltage stress on switches cannot be reduced by changing the dc-bus voltage according to the running speed.

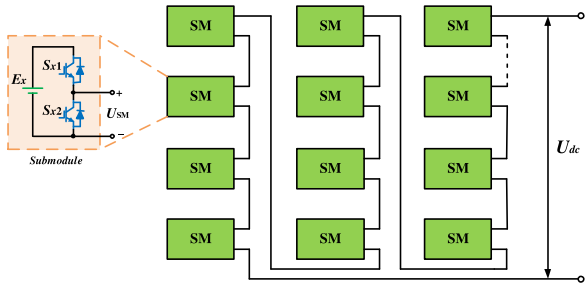

Fig. 3. Developed MMC with decentralized BESS.

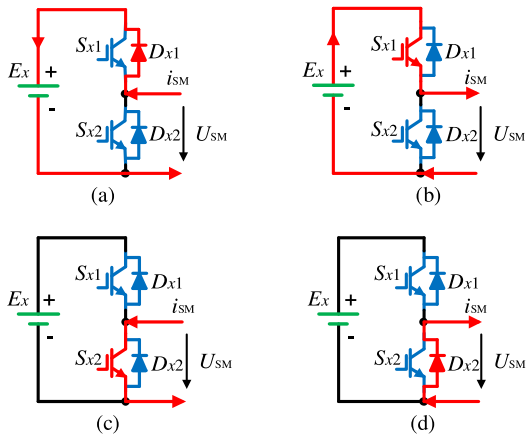

Fig. 4. Operation states of a two-level SM. (a) Charging mode. (b) Discharging mode. (c) Bypass mode 1. (d) Bypass mode 2.

The multilevel phase voltage cannot be achieved, which limits the output torque in high-speed operations. Also, the fault tolerance for battery cells and flexible charging functions are not achieved. This paper proposes an MMC-based SRM drive with decentralized battery energy storage system (BESS) for HEVs. Compared to conventional and existing SRM drives, the presented topology has several advantages, including flexible dc-bus voltage, multilevel phase voltage, modular structure, fault-tolerance ability for battery cells, flexible running charging, grid-connecting charging, and SOC balancing capability, which will be analyzed in detail in the following.

III. Proposed MMC-Based SRM Drive With Decentralized BESS

A. Proposed MMC-Based SRM Drive

Fig. 3 shows the developed MMC with decentralized BESS. A half-bridge converter and a battery pack E_x are employed as an SM, and each SM is made up of two insulated-gate bipolar transistors (IGBTs), including an upper switch S_{x1} and a lower switch S_{x2}. The output voltage of each SM is $U_{\rm SM}$, which is determined by the SM working state according to the ON–OFF state of two switches, and multiple SMs are connected in series to form a decentralized BESS for the total dc-bus voltage $U_{\rm dc}$. In this configuration, battery cells are decentralized by individual SMs and each battery cell SM can be controlled independently.

As shown in Fig. 4, each SM is a two-level half-bridge converter consisting of a battery cell and two switches. In the IGBT,

TABLE I
SM OPERATION STATES

SM state	S_{x1}	S_{x2}	D_{x1}	D_{x2}	U_{sm}	i_{sm}	E_x
On	On	Off	Off	Off	U_{by}	Positive	Discharging mode
On	Off	Off	On	Off	$-U_{by}$	Negative	Charging mode
Off	Off	On	Off	Off	0	Negative	Bypass mode 1
Off	Off	Off	Off	On	0	Positive	Bypass mode 2

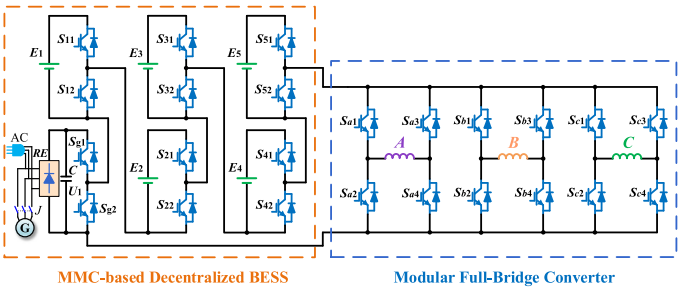

Fig. 5. MMC-based SRM drive with six SMs for HEVs.

there is an integrated antiparallel diode. The state of the antiparallel diode is defined as ON when there is a current flowing through it, and is defined as OFF with no current. The operation states of the two-level SM under different IGBT switching states are shown in Fig. 4 and Table I.

According to the SM working states, the switching function of SMs can be expressed by

$$U_{\rm SM} = \begin{cases} U_{\rm by}, & S_{x1} \text{ is ON}, S_{x2} \text{ is OFF}, D_{x1} \text{ is OFF}, D_{x2} \text{ is OFF} \\ -U_{\rm by}, & S_{x1} \text{ is OFF}, S_{x2} \text{ is OFF}, D_{x1} \text{is ON}, D_{x2} \text{ is OFF} \\ 0, & S_{x1} \text{ is OFF}, S_{x2} \text{ is ON}, D_{x1} \text{ is OFF}, D_{x2} \text{ is OFF} \\ 0, & S_{x1} \text{ is OFF}, S_{x2} \text{ is OFF}, D_{x1} \text{ is OFF}, D_{x2} \text{ is ON}. \end{cases} \tag{4}$$

The dc-bus voltage is the sum of the SM output voltages, which is given by

$$U_{\rm dc} = NU_{\rm SM} \tag{5}$$

where N is the number of total SMs.

In order to illustrate the functions of the proposed drive more clearly, a simplified system with six SMs is adopted as an example in this paper for analysis. Fig. 5 shows an MMC-based SRM drive with six SMs for HEV applications, including an MMC-based decentralized BESS and a modular full-bridge converter. The full-bridge converter is used to achieve a completely modular converter structure, where the commercial power modules can be directly used for the proposed drive, which is beneficial for the market mass production [42]–[44]. Furthermore, the full-bridge converter can also provide a flexible fault-tolerant operation for power switch faults with bipolar excitation [42], [43], which is suitable for high-performance and safety-critical vehicle applications. The MMC is composed of six SMs by using IGBTs with integrated fast recovery antiparallel diode, an energy storage unit including five battery packs $(E_1$–$E_5)$, and a GCU including a generator (G), a relay (J), a rectifier (RE), and a capacitor (C). In the modular full-bridge converter, six half-bridge modules are used to drive the three-phase SRM, where two half-bridge modules are employed for one phase, which achieves a completely modular structure for massive production. By employing the proposed SRM drive, multiple working modes can be flexibly achieved and the system performance can be improved.

A BESS for EVs is composed of several battery packs connected in series to satisfy a voltage and capacity specification [45], [46]. Therefore, each battery pack can be easily connected with a converter for independent control [47], [48]. For MMC topologies, the battery packs can be connected with MMC SMs for conventional AC motor drives in EVs [39], [49], [50], allowing high flexibility for the discharge and charge of each battery pack. In these papers, to reduce the complexity of the converter circuit for analysis, four to six SMs are usually adopted for the phases for the proof of concept. Therefore, in this paper, in order to explain the principle of the proposed SRM drive more clearly with reduced complexity, six SMs connecting with five battery packs and a GCU are just adopted for analysis and experiments. However, MMCs show excellent expansibility [39], [49], [50]. Hence, more flexible dc-bus voltage, multilevel voltage, battery discharging and charging, and battery fault-tolerance ability can be further achieved by employing more battery SMs for the proposed SRM system.

B. Battery Driving Mode

1) Full Battery Cells Driving: When relay J is OFF and switch S_{g2} is ON, the GCU SM is bypassed and the proposed SRM drive can work in pure-battery driving mode. Under this condition, the dc-bus voltage can be flexibly controlled by employing different SMs. Fig. 6 shows the working stages of the motor drive in battery driving mode with flexible excitation and demagnetization voltages.

Fig. 6(a) shows the condition that E_1–E_5 are all employed for excitation, where switches S_{11}, S_{21}, S_{31}, S_{41}, and S_{51} are all turned ON, and S_{12}, S_{22}, S_{32}, S_{42}, and S_{52} are all kept OFF for the phase winding excitation; in the winding demagnetization mode, the current flows back to the power source through S_{11}, S_{21}, S_{31}, S_{41}, and S_{51}, as shown in Fig. 6(b). For this condition, the discharging and charging voltages for the dc link are given by

$$U_{\rm dc} = \begin{cases} 5U_{\rm SM}, & \text{Discharging state} \\ 5U_{\rm SM}, & \text{Charging state.} \end{cases} \tag{6}$$

The phase A voltage is directly the dc-bus voltage under this condition, which can be expressed as

$$U_a = \begin{cases} 5U_{\rm SM}, & \text{Phase A excitation} \\ -5U_{\rm SM}, & \text{Phase A demagnetization.} \end{cases} \tag{7}$$

2) Two Battery Cells Driving With Two Additional Battery Cells Charging: Fig. 6(c) and (d) shows the conditions that two battery cells are employed for the winding excitation, and

additional two SMs are employed to improve the voltage for winding demagnetization and achieve battery charging during running conditions. For example, E_1 and E_2 are used to supply the power to the motor, and E_3 and E_4 are employed to increase the demagnetization voltage, where S_{11} and S_{21} are both turned ON, and S_{52} is also turned ON to bypass the E_5 SM. In the excitation mode of phase A, the current flows through S_{11} and S_{21}, the diodes in S_{32} and S_{42}, and the bypass switch S_{52} to the phase A converter, as shown in Fig. 6(c); when phase A is turned OFF, the demagnetization current goes through the bypass switch S_{52}, the diodes in S_{31} and S_{41}, and switches S_{11} and S_{21} to the power source, as shown in Fig. 6(d). The demagnetization voltage is elevated by E_3 and E_4, where the multilevel phase voltage can be achieved to accelerate both the excitation and demagnetization processes for torque improvements, and also E_3 and E_4 can be charged by the demagnetization current. Under this condition, the charging and discharging voltages for the dc link are given by

$$U_{\rm dc} = \begin{cases} 2U_{\rm SM}, & \text{Discharging state} \\ 4U_{\rm SM}, & \text{Charging state.} \end{cases} \tag{8}$$

The phase A demagnetization voltage is directly increased to $-4U_{\rm SM}$ due to additional battery cells charging. Although the dc-bus voltage is only $2U_{\rm SM}$ in the discharging mode, the excitation voltage of phase A can still be elevated to $4U_{\rm SM}$ by phase C demagnetization, according to the current overlapping states [24], [29]. When the phase C current is larger than the phase A current in the phase C demagnetization stage, the phase C winding works as a current source to supply the current to phase A and simultaneously charge the battery. Because the phase C winding is under the demagnetization voltage $-4U_{\rm SM}$ due to the battery cell E_3 and E_4 charging, the phase A voltage can be elevated to $4U_{\rm SM}$ when the phase C winding supplies the current to phase A. When the phase C current decreases to be smaller than phase A current, the dc-link power source and phase C both supply the current to phase A, and the phase A voltage returns to $2U_{\rm SM}$. Hence, after the excitation current quickly established at the beginning of the turn-ON region with an increased voltage, the phase voltage can immediately decrease to the power supply voltage in the main turn-ON region, which not only improves the torque, but also achieves a lower excitation voltage.

Therefore, multilevel phase voltage is achieved in the proposed drive and the phase A voltage can be expressed as, eq. (9) as shown at the bottom of this page.

3) One Battery Cell Driving With Two Additional Battery Cells Charging: Fig. 6(e) and (f) illustrates that only E_1 is employed to supply the power, and E_2 and E_5 are used for charging, where S_{11} is turned ON, and S_{32} and S_{42} are also turned ON to bypass E_3 and E_4. When phase A is in the turn-ON region, E_1 provides the current flowing through switch S_{11}, the diodes of S_{22} and S_{52}, and switches S_{32} and S_{42}, as shown in Fig. 6(e); when phase A is turned OFF, the current goes back to the power supply through S_{42} and S_{32}, the diodes of S_{51} and S_{21}, and switch S_{11}, as shown in Fig. 6(f). Under this condition, E_2 and E_5 are employed to additionally increase the demagnetization voltage, which are also charged by the demagnetization current. The discharging and charging voltages for the dc link under this condition are given by

$$U_{\rm dc} = \begin{cases} U_{\rm SM}, & \text{Discharging state} \\ 3U_{\rm SM}, & \text{Charging state.} \end{cases} \tag{10}$$

Similarly, the phase A voltage can be expressed as follows: eq. (11) as shown at the bottom of this page.

Therefore, in the pure-battery driving mode, by controlling the switches in SMs, the battery cells can be flexibly selected for both excitation and demagnetization, and the dc-bus voltage can be flexibly controlled according to low-speed and high-speed operations. In the phase turn-ON region, k_1 SMs can be put into use for excitation, as shown in Fig. 7(a); while additional k_2 SMs can be used to increase the demagnetization voltage and achieve battery charging in the phase turn-OFF region, as shown in Fig. 7(b). For idle battery cells, the lower switches in corresponding SMs are turned ON to make the SMs work in bypass mode; for the battery cells that used to enhance the demagnetization voltage for the torque improvement, the demagnetization current can flow through upper switches in SMs to achieve battery charging. Battery SOC can be balanced by employing the higher-SOC battery cell for discharging and the lower-SOC battery cell for charging. The discharging and charging voltages for the dc link can be expressed as

$$U_{\rm dc} = \begin{cases} k_1 U_{\rm SM}, & \text{Discharging state} \\ (k_1 + k_2) U_{\rm SM}, & \text{Charging state.} \end{cases} \tag{12}$$

Taking phase A for example, the phase A demagnetization voltage is directly increased due to additional battery cell charging. The phase A excitation voltage can also be elevated by the phase C demagnetization, according to the current overlapping state. The phase A voltage in battery driving mode is given by eq. (13) as shown at the bottom of this page.

C. GCU Driving Mode

When relay *J* is ON and switch S_{g2} is OFF, the GCU SM is put into use and the proposed SRM drive can work in GCU driving

$$U_a = \begin{cases} 4U_{\rm SM}, & \text{Phase A excitation, Phase C demagnetization}, i_c > i_a \\ 2U_{\rm SM}, & \text{Phase A excitation, Phase C demagnetization}, i_c < i_a \\ -4U_{\rm SM}, & \text{Phase A demagnetization, Phase B excitation}, i_a > i_b \\ -2U_{\rm SM}, & \text{Phase A demagnetization, Phase B excitation}, i_a < i_b \\ -4U_{\rm SM}, & \text{Phase A demagnetization, Phase B in ZVL}, i_a < i_b \end{cases} \tag{9}$$

mode. In this mode, only GCU is used for excitation, while the multilevel phase voltage can also be achieved, and the demagnetization voltage can be increased and flexibly controlled by employing different SMs. Fig. 8 shows the working stages of the drive in GCU driving mode with flexible demagnetization voltages. In the phase turn-ON region, the single GCU provides the power for the phase winding excitation, as shown in Fig. 8(a) while additional k_2 SMs can be employed to increase the demagnetization voltage and achieve battery charging in the phase turn-OFF region, as shown in Fig. 8(b). Also, in the demagnetization mode, the lower-SOC battery cell can be employed for charging to balance the battery SOC. The charging and discharging voltages for the dc link in GCU driving mode can be expressed in terms of the GCU and SM-output voltages as

$$U_{\rm dc}=\begin{cases}U_g, & \text{Discharging state}\\ -U_g-k_2U_{\rm SM}, & \text{Charging state.}\end{cases} \tag{14}$$

Similarly, the phase A voltage in GCU driving mode can be expressed as follows: eq. (15) as shown at the bottom of this page.

D. GCU-Battery Driving Mode

When relay *J* is ON and switch S_{g2} is OFF, the GCU is put into use, and simultaneously, the battery SMs can also be employed to assist the GCU to work in the GCU-battery driving mode. In this situation, the GCU and battery cells are used as a hybrid power source for both excitation and demagnetization. The multilevel phase voltage can be achieved by charging the idle SMs and the demagnetization voltage is increased to improve the torque, which is similar to the battery driving mode, where the only difference is that the GCU is used. In the winding excitation mode, the GCU and k_1 battery SMs work together to supply the power to the motor, as shown in Fig. 9(a); in the winding demagnetization mode, additional k_2 battery SMs can be employed for charging, as shown in Fig. 9(b), which elevate the demagnetization voltage. The charging battery cells can be flexibly selected according to the battery SOC. The charging and discharging voltages for the dc link in the hybrid-source mode can be expressed as

$$U_{\rm dc}=\begin{cases}U_g+k_1U_{\rm SM}, & \text{Discharging state}\\ U_g+(k_1+k_2)U_{\rm SM}, & \text{Charging state.}\end{cases} \tag{16}$$

Similarly, the phase A voltage in hybrid-source mode can be expressed as follows: eq. (17) as shown at the bottom of the next page.

E. Standstill Charging Mode

Under standstill conditions, the battery cells can be flexibly charged from the GCU or grids. There are two steps to achieve the battery charging. First, the switches of phases A, B, and C are all turned ON simultaneously for the winding excitation; second, these switches are all turned OFF simultaneously to make the phase currents flow back to the dc source. Fig. 10(a) shows the condition that the windings are excited by the rectification from GCU/grids, where S_{g1} is turned ON. When switches S_{a1} and S_{a4}, S_{b1} and S_{b4}, S_{c1} and S_{c4} are all turned ON, the current goes from capacitor *C* through switch S_{g1} and the diodes of S_{12}, S_{22}, S_{32}, S_{42}, and S_{52} to the full-bridge converter, and the energy is stored in the three-phase windings. Then, switches S_{a1} and S_{a4}, S_{b1} and S_{b4}, and S_{c1} and S_{c4} are all turned OFF, and the current goes from phase windings through the diodes of S_{11}, S_{21}, S_{31}, S_{41}, S_{51}, and switch Sg_2 to the battery cells E_1–E_5, where full-battery cell charging is achieved, as shown in Fig. 10(b). However, each battery cell can be flexibly selected for charging according to the battery SOC. For example, S_{42} and S_{52} can be turned ON to bypass E_4 and E_5 during the charging process, where only E_1, E_2, and E_3 are employed for charging, as shown in Fig. 10(c).

There are two operation modes for the battery charging, including the phase current continuous mode and phase current discontinuous mode, which are determined by the duty cycle and the switching frequency of driving signals for the full-bridge converter. In the phase current continuous mode, the discharging

$$U_a=\begin{cases}3U_{\rm SM}, & \text{Phase A excitation, Phase C demagnetization, } i_c>i_a\\ U_{\rm SM}, & \text{Phase A excitation, Phase C demagnetization, } i_c<i_a\\ -3U_{\rm SM}, & \text{Phase A demagnetization, Phase B excitation, } i_a>i_b\\ -U_{\rm SM}, & \text{Phase A demagnetization, Phase B excitation, } i_a<i_b\\ -3U_{\rm SM}, & \text{Phase A demagnetization, Phase B in ZVL, } i_a<i_b\end{cases} \tag{11}$$

$$U_a=\begin{cases}(k_1+k_2)U_{\rm SM}, & \text{Phase A excitation, Phase C demagnetization, } i_c>i_a\\ k_1U_{\rm SM}, & \text{Phase A excitation, Phase C demagnetization, } i_c<i_a\\ -(k_1+k_2)U_{\rm SM}, & \text{Phase A demagnetization, Phase B excitation, } i_a>i_b\\ -k_1U_{\rm SM}, & \text{Phase A demagnetization, Phase B excitation, } i_a<i_b\\ -(k_1+k_2)U_{\rm SM}, & \text{Phase A demagnetization, Phase B in ZVL, } i_a<i_b\end{cases} \tag{13}$$

and charging currents by employing one phase can be expressed according to different stages as

$$i_{k\mathrm{by}}(t)=\begin{cases} I_{k0}+\dfrac{I_{km}-I_{k0}}{DT_s}t, & 0\le t\le DT_s \\ I_{km}-\dfrac{I_{km}-I_{k0}}{(1-D)T_s}(t-DT_s), & DT_s<t\le T_s \end{cases} \tag{18}$$

where I_{k0} is the initial phase current, I_{km} is the maximum phase current, and D and T_s are the switching period and duty cycle of the pulsewidth modulation (PWM) signal, respectively.

When three-phase windings are all used for charging, the sum of the maximum and minimum currents flowing through the phase windings are given by

$$\begin{cases} I_{\max}=I_{am}+I_{bm}+I_{cm} \\ I_{\min}=I_{a0}+I_{b0}+I_{c0}. \end{cases} \tag{19}$$

Hence, the discharging and charging currents with three phases are expressed as

$$i_{\mathrm{by}}(t)=\begin{cases} I_{\min}+\dfrac{I_{\max}-I_{\min}}{DT_s}t, & 0\le t\le DT_s \\ I_{\max}-\dfrac{I_{\max}-I_{\min}}{(1-D)T_s}(t-DT_s), & DT_s<t\le T_s. \end{cases} \tag{20}$$

In the phase current discontinuous mode, considering the discontinuous current, the discharging and charging currents are expressed as

$$i_{\mathrm{by}}(t)=\begin{cases} I_{\min}+\dfrac{I_{\max}-I_{\min}}{DT_s}t, & 0\le t\le DT_s \\ I_{\max}-\dfrac{I_{\max}-I_{\min}}{(1-D)T_s}(t-DT), & DT_s<t\le T_0 \\ 0, & T_0<t\le T_s \end{cases} \tag{21}$$

where T_0 is the charging current ending period.

F. Battery Fault-Tolerance Mode

A battery system may consist of many battery cells, and each battery cell has a normal operating mode and would also be subject to faults. Serious conditions, such as high heat generation, overcharge or overdischarge event, and aging of the battery, would result in battery faults and cause irreversible and catastrophic damages during the vehicle running process [51]–[54]. When serious battery faults occur, the HEV will work under unsafe conditions if the faulty ones are still used. However, if the faulty battery cells can be bypassed through control, it will significantly increase the reliability of the whole system. Hence, a fault-tolerance method for the battery system is much important in safety-critical vehicle applications.

The proposed SRM drive can provide flexible fault-tolerance control for the battery system. In the battery driving mode, if E_5 has a fault, switch S_{52} can be turned ON to bypass E_5, and the current will flow through S_{52} instead of E_5, as shown in Fig. 11(a). Also, the charging current will not go through E_5 due to turning ON S_{52}. Hence, the faulty cell E_5 can be easily bypassed by controlling the switch in the corresponding SM. In the GCU-battery driving mode, if E_4 and E_5 both have faults, switches S_{42} and S_{52} can be turned ON to bypass E_4 and E_5, and the current will directly go through S_{42} and S_{52}, as shown in Fig. 11(b). Therefore, the battery fault tolerance can be flexibly achieved under both driving and charging conditions under different working modes.

G. Comparison With Existing Topologies

Fig. 12 shows a qualitative comparison of the proposed MMC-based SRM drive and existing topologies for electric powertrain systems, which shows a superior overall performance. In the figure, the highest score for each item will be obtained if the dc-bus voltage can be flexibly controlled at multiple values, a completely modular structure for the converter can be achieved by using commercial power modules, each faulty battery pack can be easily bypassed, the battery can be flexibly charged by connecting the grid, each phase is totally isolated

$$U_a=\begin{cases} U_g+k_2U_{\mathrm{SM}}, & \text{Phase A excitation, Phase C demagnetization, } i_c>i_a \\ U_g, & \text{Phase A excitation, Phase C demagnetization, } i_c<i_a \\ -U_g-k_2U_{\mathrm{SM}}, & \text{Phase A demagnetization, Phase B excitation, } i_a>i_b \\ -U_g, & \text{Phase A demagnetization, Phase B excitation, } i_a<i_b \\ -U_g-k_2U_{\mathrm{SM}}, & \text{Phase A demagnetization, Phase B in ZVL, } i_a<i_b. \end{cases} \tag{15}$$

$$U_a=\begin{cases} U_g+(k_1+k_2)U_{\mathrm{SM}}, & \text{Phase A excitation, Phase C demagnetization, } i_c>i_a \\ U_g+k_1U_{\mathrm{SM}}, & \text{Phase A excitation, Phase C demagnetization, } i_c<i_a \\ -U_g-(k_1+k_2)U_{\mathrm{SM}}, & \text{Phase A demagnetization, Phase B excitation, } i_a>i_b \\ -U_g-k_1U_{\mathrm{SM}}, & \text{Phase A demagnetization, Phase B excitation, } i_a<i_b \\ -U_g-(k_1+k_2)U_{\mathrm{SM}}, & \text{Phase A demagnetization, Phase B in ZVL, } i_a<i_b \end{cases} \tag{17}$$

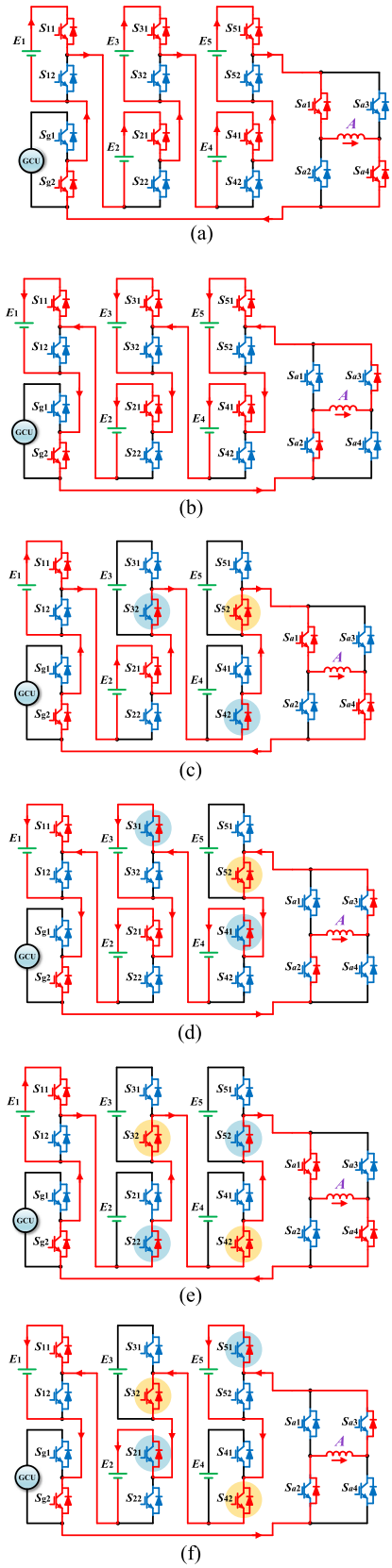

Fig. 6. Battery driving mode by employing different SMs. (a) E_1–E_5 are all employed for excitation. (b) E_1–E_5 are all employed for demagnetization. (c) E_1 and E_2 are employed for excitation. (d) E_1, E_2, E_3, and E_4 are employed for demagnetization. (e) E_1 is employed for excitation. (f) E_1, E_2, and E_5 are employed for demagnetization.

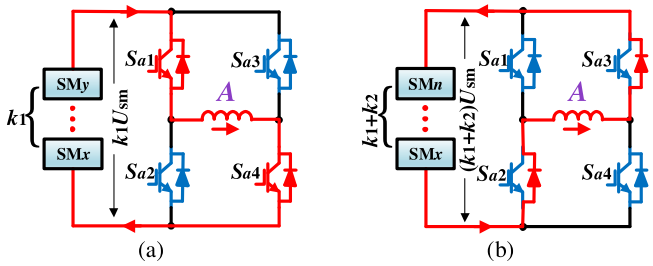

Fig. 7. Battery driving mode with flexible multilevel voltage and battery charging. (a) Excitation. (b) Demagnetization and battery charging.

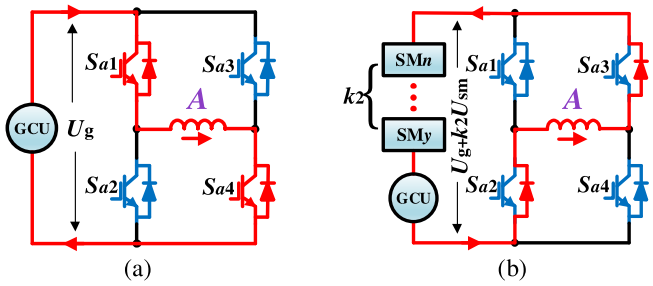

Fig. 8. GCU driving mode with flexible multilevel voltage and battery charging. (a) Excitation. (b) Demagnetization and battery charging.

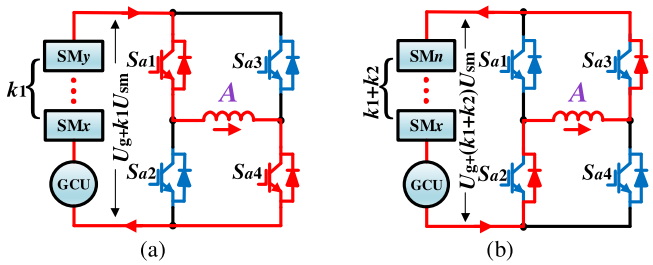

Fig. 9. GCU-battery driving mode with flexible multilevel voltage and battery charging. (a) Excitation. (b) Demagnetization and battery charging.

and can be independently controlled, and different multilevel voltages can be flexibly achieved and regulated. Otherwise, a lower score will be given.

For the conventional asymmetrical half-bridge converter, the dc-bus voltage is fixed and the multilevel voltage cannot be achieved, which limit the torque capability in high-speed operations; the dc-bus voltage cannot be changed according to the speed to reduce the voltage stress and switching loss; battery fault-tolerance and charging abilities are not equipped; modular structure is not obtained due to the special converter configuration. To achieve the multilevel voltage, four-level converters are proposed in [23] and [24]. Although an additional charge capacitor is employed to increase the phase voltage in the excitation and demagnetization regions, other limitations still exist, which are similar to the asymmetrical converter. To achieve battery charging, modified C-dump converters are presented in [27] and [28]. However, the fault-tolerance ability is poor because three phases are not isolated in the circuit, and flexible dc-bus voltage and modular structure cannot be achieved. In [29]

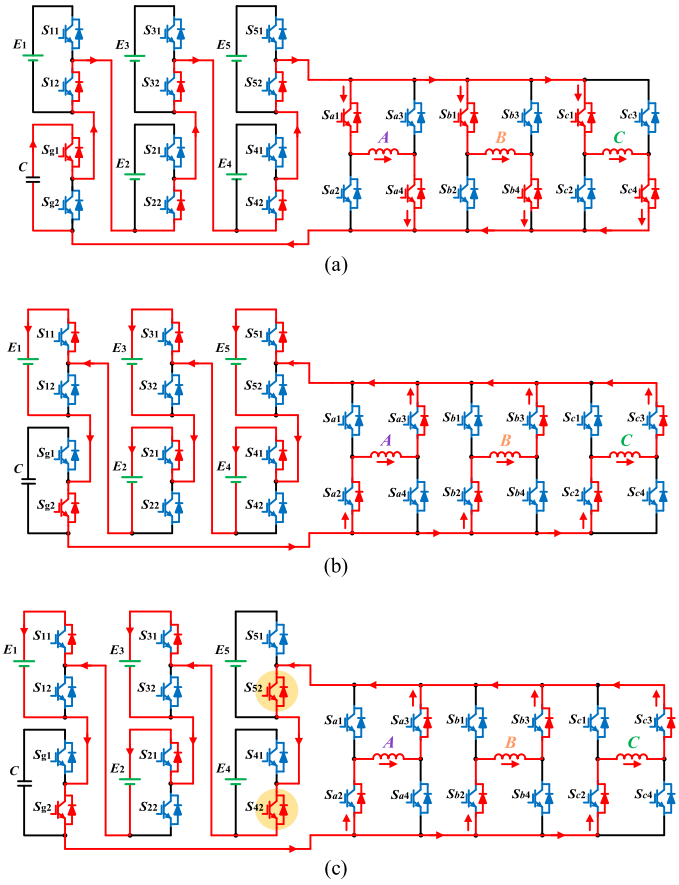

Fig. 10. Battery charging under standstill condition. (a) Winding excitation by the rectification from GCU/grids. (b) E_1–E_5 charging from GCU/grids. (c) E_1, E_2, and E_3 charging from GCU/grids.

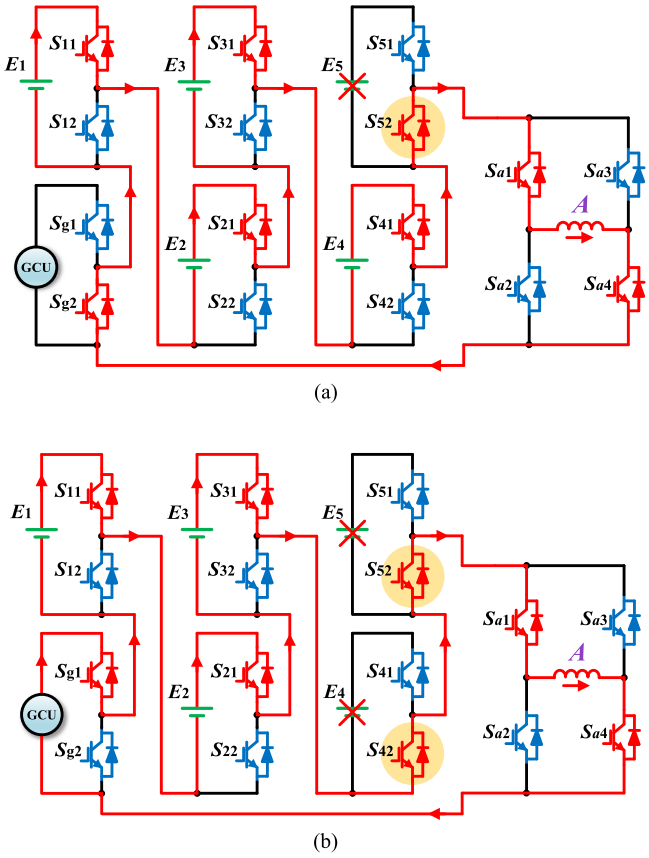

Fig. 11. Battery fault-tolerance control. (a) Battery driving mode with E_5 fault. (b) GCU-battery driving mode with E_4 and E_5 faults.

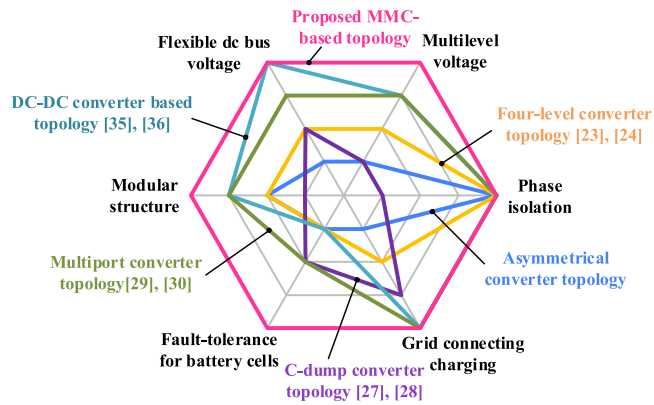

Fig. 12. Qualitative comparison of proposed and existing SRM drive topologies.

and [30], multiport converters are presented to achieve battery charging, multilevel voltage, and flexible driving control. However, flexible dc-bus voltage, fault tolerance for battery cells, and completely modular structure are not achieved. In order to obtain a flexible dc-bus voltage and battery charging ability, a dc–dc converter is employed in the front end of SRM drives [35], [36]. However, additional inductors and capacitors are required, and multilevel voltage, modular structure, and battery fault-tolerance ability are not achieved.

Compared to existing topologies, the MMC is employed for the SRM drive in this paper, where the battery cells are decentralized by the SMs. Standard half-bridge modules are used for both the MMC and the full-bridge converter in the proposed motor drive and, thus, has a good fault-tolerance ability due to phase isolation and achieves a completely modular structure. Multiple modes/functions can be flexibly achieved by controlling the MMC-based drive, including the battery driving mode, GCU driving mode, GCU-battery driving mode, running charging mode, standstill charging mode, and battery fault-tolerance mode. By using the MMC, flexible dc-bus voltage is achieved, which can reduce the voltage stress and switching loss on the switches according to the running speed. The reliability of the motor drive can also be improved due to a lower voltage stress. Multilevel phase voltage is obtained in the GCU driving mode, battery driving mode, and hybrid source driving mode, where the torque capability can be improved accordingly. Also, flexible fault-tolerance ability for battery cells is equipped by controlling the switches in corresponding SMs. Furthermore, the battery can be charged under both running and standstill conditions by utilizing the proposed converter without external ones. Battery SOC balance can be easily achieved by selecting the charged battery cells according to the SOC level.

TABLE II
MOTOR PARAMETERS

Parameters	Value
Phase number	3
Stator/rotor poles	12/8
Rated power (W)	750
Rated speed (r/min)	1500
Phase resistor (Ω)	3.01
Minimum phase inductance (mH)	27.2
Maximum phase inductance (mH)	256.7
Rotor outer diameter (mm)	55
Rotor inner diameter (mm)	30
Stator outer diameter (mm)	102.5
Stator inner diameter (mm)	55.5
Stack length (mm)	80
Stator arc angle (deg)	14
Rotor arc angle (deg)	16

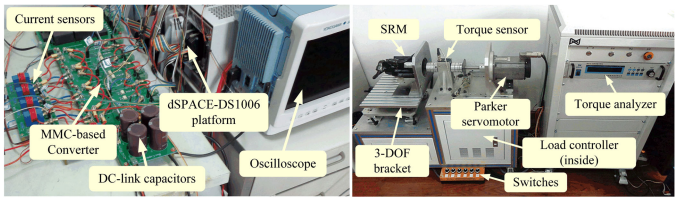

Fig. 13. Experimental setup.

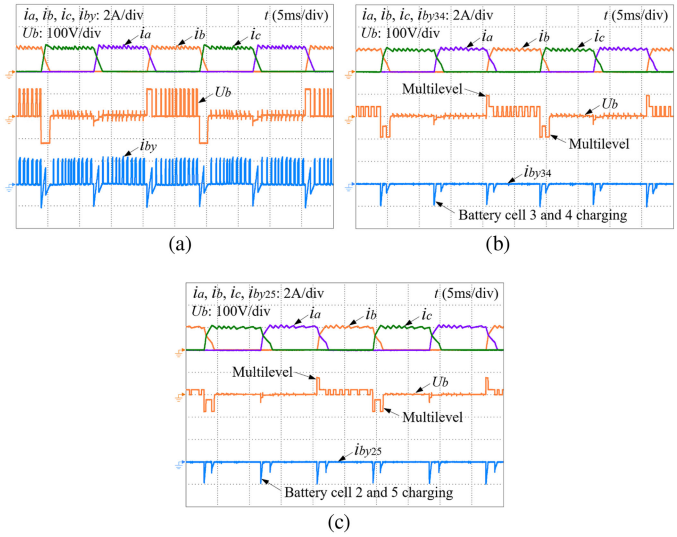

Fig. 14. Battery driving mode at low speed. (a) Driven by full voltage. (b) Driven by E_1 and E_2 with E_3 and E_4 charging. (c) Driven by E_1 with E_2 and E_5 charging.

IV. EXPERIMENTAL VERIFICATION

To verify the effectiveness of the proposed MMC-based SRM drive, experiments are carried out on a scale-down three-phase 12/8 SRM prototype by employing six SMs for proof of concept. Table II gives the main parameters of the SRM. The experimental setup is shown in Fig. 13, including the controller, power electronics, and motor test bed. The control algorithm is implemented in a dSPACE-DS1006 platform. The phase currents are detected by Hall effect current sensors LA-55P for current regulation control. A proportional integral controller is employed to implement the closed-loop speed control and the current hysteresis control method is used for phase current regulation. A multichannel isolated oscilloscope is employed to observe the voltage and current waveforms. In the motor test bed, a Parker ac servomotor is used as the load, which can be controlled by a load controller inside the cabinet. A 3-DOF bracket can be adjusted to ensure a balanced connection between the SRM and the load motor. A high-precision torque sensor (Lorenz 0261Due) is used to detect the instantaneous output torque. A 2500-line incremental encoder (ZZU4809) is installed on the motor bearing to detect the rotor position and calculate the rotational speed. A programmable dc power source is utilized to simulate the GCU part. Five 24-V battery packs are employed for the MMC configuration.

Fig. 14 shows the experimental waveforms in the battery driving mode at low speed of 300 r/min and 2-N·m load, where i_a, i_b, and i_c are the currents of phases A, B, and C, respectively, U_a is the phase A voltage, $i_{\rm by}$ is the battery current flowing through full cells, and $i_{{\rm by}x}$ is the battery current flowing through cell x. When all the battery cells are put into use, the excitation and demagnetization voltages on the phase winding are both the full-battery voltage, and the battery cells are charged and discharged alternately in each current period, as shown in Fig. 14(a). When parts of the battery cells are employed as a lower voltage power supply, the motor drive can work under multilevel phase voltage by additional battery charging during the demagnetization process, where running charging is achieved. As shown in Fig. 14(b), E_1 and E_2 are employed to supply the power, and E_3 and E_4 are used for additional charging. The demagnetization voltage of phase A is directly elevated by E_3 and E_4 charging; the excitation voltage of phase A is also increased in phase A and phase C current overlapping region, when the demagnetization current of phase C is larger than the excitation current of phase A. Due to the multilevel voltage, the excitation and demagnetization processes are both accelerated. Battery cells E_3 and E_4 are charged by the demagnetization current of each phase. In Fig. 14(c), E_1 is employed as the power supply, and E_2 and E_5 are used for additional charging, where multilevel phase voltage is also achieved. Therefore, in the battery driving mode, the dc-bus voltage can be flexibly changed according to the requirement, the voltage stress on the switches can be dramatically reduced, and the battery cells can be flexibly selected for additional charging during the demagnetization process according to the SOC level. Hence, the energy can be transferred among the battery cells to achieve the SOC balance.

Fig. 15 illustrates the experimental waveforms in the GCU driving mode at 1750 r/min. When the motor is driven by the GCU without additional battery charging, the phase voltage is directly the GCU-output voltage both in the excitation and demagnetization processes, as shown in Fig. 15(a). However, when additional battery charging is employed in the demagnetization process, as shown in Fig. 15(b), multilevel phase voltage is achieved and the battery SOC can be balanced by controlling the charging cells. The experimental results in the GCU-battery hybrid source driving mode with and without additional battery charging at 2100 and 2250 r/min are shown in Fig. 16(a) and

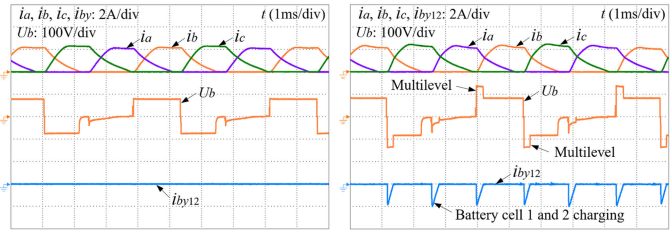

Fig. 15. GCU driving mode at high speed. (a) Driven by GCU without additional battery charging. (b) Driven by GCU with E_1 and E_2 charging.

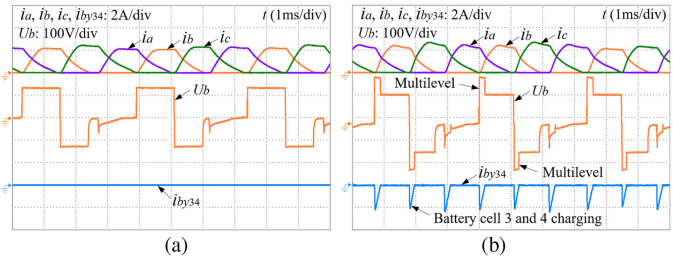

Fig. 16. GCU-battery driving mode at high speed. (a) Driven by GCU, E_1, and E_2 without additional battery charging. (b) Driven by GCU, E_1, and E_2 with E_3 and E_4 charging.

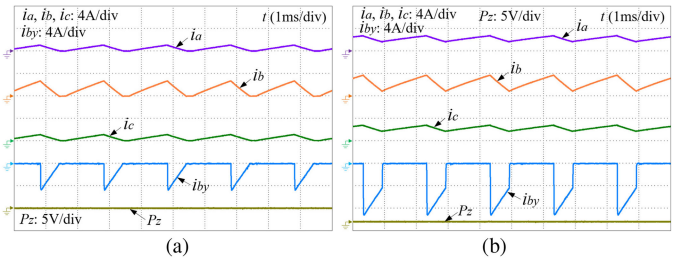

Fig. 17. Standstill battery charging mode. (a) Phase current discontinuous mode. (b) Phase current continuous mode.

(b), respectively. Similarly, the phase voltage can also be elevated by additional battery charging and the dc-bus voltage can be flexibly changed by employing different cells for excitation according to the running speed.

Under standstill conditions, the battery can also be flexibly charged from GCU/grids through the proposed drive, as shown in Fig. 17, where P_Z is the encoder output signal. PWM signals are applied to the switches in the full-bridge converter for the battery charging. In the high level of the PWM, corresponding switches for each phase are turned ON, and capacitor C supplies the power to three-phase windings, simultaneously; in the low level of the PWM, the related switches are all turned OFF, and the energy stored in phase windings feeds back to the power source and charges the battery. Fig. 17 shows the waveforms when the phase current is discontinuous and continuous by employing all battery cells for charging, where the duty cycle is 0.6 and 0.7, respectively. The encoder output signal stays at zero, and thus, the charging scheme does not lead to motor movement. The battery cells can be flexibly selected for charging or bypassed by controlling the switches in the SMs.

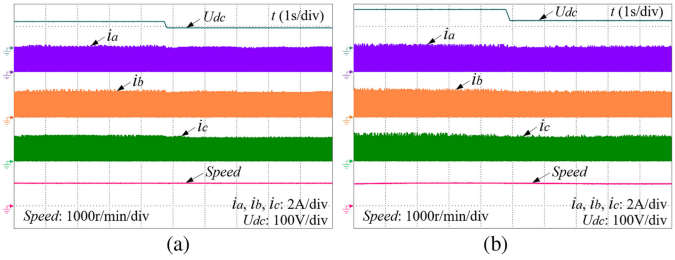

Fig. 18. Battery fault-tolerance mode. (a) Voltage step in battery driving mode with full cells when E_5 is bypassed. (b) Voltage step in GCU-battery driving mode with GCU and E_1–E_4 when E_3 and E_4 are bypassed.

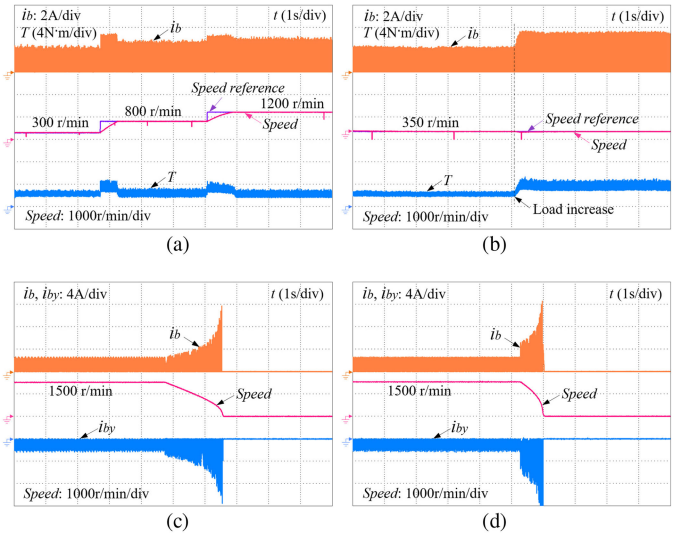

Fig. 19. Dynamic performance. (a) Speed step change. (b) Load step change. (c) Braking with turn-ON angle 20° and turn-OFF angle 30°. (d) Braking with turn-ON angle 20° and turn-OFF angle 40°.

In the battery fault-tolerance mode, the faulty battery cells can be easily bypassed by controlling the switches in SMs. Fig. 18(a) shows the voltage step in the battery driving mode with full cells when E_5 is bypassed, where the bus voltage changes from 120 to 96 V. Fig. 18(b) shows the voltage step in the hybrid source driving mode with GCU and E_1–E_4 when E_3 and E_4 are bypassed, where the bus voltage changes from 176 to 128 V. Clearly, there is no obvious fluctuation on the phase currents and speed, and the system can be steadily controlled during the transient process.

In order to investigate the dynamic performance of the proposed SRM drive, Fig. 19 shows the experimental waveforms under the speed step change, load step change, and braking conditions. As shown in Fig. 19(a), when the speed reference changes from 300 to 800 r/min and 800 to 1200 r/min with a 2-N·m load, the instantaneous speed quickly tracks the given reference and follows the reference well. When a load step from 2 to 4 N·m is applied, the instantaneous speed is still stabilized in a very short time, as shown in Fig. 19(b). In the braking process, the battery can be directly charged by the braking current, where the turn-ON and turn-OFF angles can be adjusted to achieve the flexible braking performance. When the turn-ON and turn-OFF angles are set to 20° and 30°, respectively, the braking process

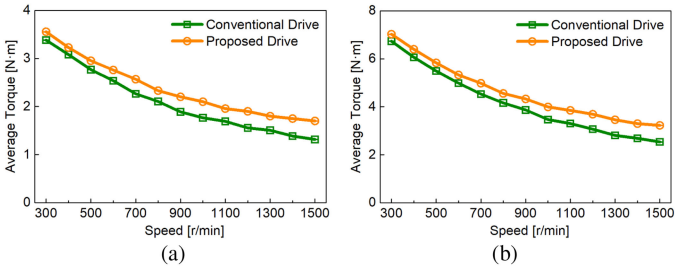

Fig. 20. Torque comparison. (a) Battery driving mode. (b) GCU driving mode.

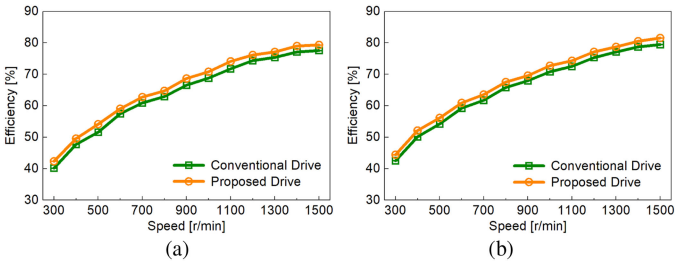

Fig. 21. Efficiency comparison. (a) Battery driving mode. (b) GCU-battery driving mode.

is finished in 2 s; while when the turn-OFF angle is extended to 40°, the braking process can be controlled within 1 s. It can be seen from the experimental results that the proposed drive has a good dynamic performance to transient changes.

Fig. 20 shows the torque comparison between the proposed MMC-based SRM drive with multilevel phase voltage and conventional drive without multilevel phase voltage in the battery driving mode and the GCU driving mode, respectively. Fig. 20(a) shows the condition that battery cells E_1 and E_2 are used to supply the power to the motor, and E_3 and E_4 are additionally employed in the demagnetization mode for multilevel voltage. Fig. 20(b) shows the condition that the GCU is used as the power source and E_1–E_4 are employed for multilevel voltage. By employing additional battery charging in the phase demagnetization mode, multilevel phase voltage can be flexibly achieved, where the winding excitation and demagnetization processed are both accelerated. The torque can be improved by 28% due to the multilevel voltage, especially in high-speed operations.

Fig. 21 shows the system efficiency comparison between the proposed and conventional drives with and without the multilevel voltage and variable dc-bus voltage. Fig. 21(a) shows the efficiency comparison in the battery driving mode with 2-N·m load and Fig. 21(b) shows the efficiency comparison in the GCU-battery driving mode with 4-N·m load. For the conventional drive, all the battery cells are employed to supply the power in both battery driving mode and hybrid source driving mode, where the multilevel voltage and variable dc-bus voltage are not achieved. In order to improve the system performance, multilevel phase voltage is achieved and the dc-bus voltage is also adjusted to a lower value according to the running speed. From the comparison, it can be seen that the system efficiency can be improved by 2% in the proposed drive due to both the multilevel voltage and variable dc-bus voltage.

It should be noted that, in order to explain the functions and operation modes of the proposed SRM drive more clearly, only six SMs are adopted in this paper for analysis and experiments. However, more flexible dc-bus voltage, battery charging, multilevel phase voltage, and battery fault-tolerance ability can be further achieved by employing more SMs for the proposed motor system.

V. Conclusion

In this paper, an MMC-based SRM drive is proposed for HEV applications, which not only improves the motor system performance with variable dc-bus and multilevel voltages, but also achieves flexible charging functions and battery fault-tolerance ability. In the proposed drive, the MMC is employed for the BESS, where battery cells are decentralized by SMs. In order to achieve a modular structure, the full-bridge converter is used to drive the motor. Multiple modes/functions can be achieved by controlling the SMs in the MMC, including the battery driving mode, GCU driving mode, GCU-battery driving mode, running charging mode, standstill charging mode, and battery fault-tolerance ability. The main contributions and advantages of this paper are as follows.

1) Flexible dc-bus voltage is achieved by selecting the working SMs according to the running speed, which can reduce the voltage stress on the switches and also improve the system reliability.
2) Multilevel phase voltage is obtained by employing additional battery cell charging in the demagnetization process, where the torque capability can be improved accordingly.
3) Modular structure is achieved by using standard half-bridge modules, which is beneficial for the market mass production.
4) Flexible charging functions are achieved, including the running charging and standstill charging. The battery can be directly charged by the demagnetization current during the running condition or braking process. Under standstill conditions, the battery can also be charged from the GCU or grids through the proposed drive without external ones.
5) Flexible fault-tolerance ability for battery cells is achieved by controlling the switch in corresponding SM.
6) Battery SOC balance can be easily achieved by selecting the charged battery cells according to the SOC level, no matter under running or standstill charging conditions.

Although this paper has targeted electrified vehicle applications, the developed technology can also be applied to other applications, such as more electric aircraft, traction drives, and electrical ships.

References

[1] S. S. Williamson, A. K. Rathore, and F. Musavi, "Industrial electronics for electric transportation: Current state-of-the-art and future challenges," *IEEE Trans. Ind. Electron.* vol. 62, no. 5, pp. 3021–3032, May 2015.
[2] A. A. Ferreira, J. A. Pomilio, G. Spiazzi, and L. de Araujo Silva, "Energy management fuzzy logic supervisory for electric vehicle power supplies system," *IEEE Trans. Power Electron.*, vol. 23, no. 1, pp. 107–115, Jan. 2008.

[3] G. Carli and S. S. Williamson, "Technical considerations on power conversion for electric and plug-in hybrid electric vehicle battery charging in photovoltaic installations," *IEEE Trans. Power Electron.*, vol. 28, no. 12, pp. 5784–5792, Dec. 2013.

[4] O. C. Onar, J. Kobayashi, and A. Khaligh, "A fully directional universal power electronic interface for EV, HEV, and PHEV applications," *IEEE Trans. Power Electron.*, vol. 28, no. 12, pp. 5489–5498, Dec. 2013.

[5] A. Emadi, Y. J. Lee, and K. Rajashekara, "Power electronics and motor drives in electric, hybrid electric, and plug-in hybrid electric vehicles," *IEEE Trans. Ind. Electron.*, vol. 55, no. 6, pp. 2237–2245, Jun. 2008.

[6] Z. Yang, F. Shang, I. P. Brown, and M. Krishnamurthy, "Comparative study of interior permanent magnet, induction, and switched reluctance motor drives for EV and HEV applications," *IEEE Trans. Transp. Electrific.*, vol. 1, no. 3, pp. 245–254, Oct. 2015.

[7] I. Boldea, L. N. Tutelea, L. Parsa, and D. Dorrell, "Automotive electric propulsion systems with reduced or no permanent magnets: An overview," *IEEE Trans. Ind. Electron.*, vol. 61, no. 10, pp. 5696–5711, Oct. 2014.

[8] M. Krishnamurthy, C. S. Edrington, A. Emadi, P. Asadi, M. Ehsani, and B. Fahimi, "Making the case for applications of switched reluctance motor technology in automotive products," *IEEE Trans. Power Electron.*, vol. 21, no. 3, pp. 659–675, May 2006.

[9] E. Bostanci, M. Moallem, A. Parsapour, and B. Fahimi, "Opportunities and challenges of switched reluctance motor drives for electric propulsion: A comparative study," *IEEE Trans. Transp. Electrific.*, vol. 3, no. 1, pp. 58–75, Mar. 2017.

[10] J. Cai and Z. Deng, "Unbalanced phase inductance adaptable rotor position sensorless scheme for switched reluctance motor," *IEEE Trans. Power Electron.*, vol. 33, no. 5, pp. 4285–4292, May 2018.

[11] A. Chiba, K. Kiyota, N. Hoshi, M. Takemoto, and S. Ogasawara, "Development of a rare-earth-free SR motor with high torque density for hybrid vehicles," *IEEE Trans. Energy Convers.*, vol. 30, no. 1, pp. 175–182, Mar. 2015.

[12] B. Bilgin, A. Emadi, and M. Krishnamurthy, "Comprehensive evaluation of the dynamic performance of a 6/10 SRM for traction application in PHEVs," *IEEE Trans. Ind. Electron.*, vol. 60, no. 7, pp. 2564–2575, Jul. 2013.

[13] J. Ye, B. Bilgin, and A. Emadi, "An extended-speed low-ripple torque control of switched reluctance motor drives," *IEEE Trans. Power Electron.*, vol. 30, no. 3, pp. 1457–1470, Mar. 2015.

[14] W. Ding, S. Yang, Y. Hu, S. Li, T. Wang, and Z. Yin, "Design consideration and evaluation of a 12/8 high-torque modular-stator hybrid excitation switched reluctance machine for EV applications," *IEEE Trans. Ind. Electron.*, vol. 64, no. 12, pp. 9221–9232, Dec. 2017.

[15] C. Gan, J. Wu, M. Shen, S. Yang, Y. Hu, and W. Cao, "Investigation of skewing effects on the vibration reduction of three-phase switched reluctance motors," *IEEE Trans. Magn.*, vol. 51, no. 9, Sep. 2015, Art. no. 8203509.

[16] M. A. Kabir and I. Husain, "Design of mutually coupled switched reluctance motors (MCSRMs) for extended speed applications using 3-phase standard inverters," *IEEE Trans. Energy Convers.*, vol. 31, no. 2, pp. 436–445, Jun. 2016.

[17] R. Martin, J. D. Widmer, B. C. Mecrow, M. Kimiabeigi, A. Mebarki, and N. L. Brown, "Electromagnetic considerations for a six-phase switched reluctance motor driven by a three-phase inverter," *IEEE Trans. Ind. Appl.*, vol. 52, no. 5, pp. 3783–3791, Sep./Oct. 2016.

[18] S. Song, Z. Xia, Z. Zhang, and W. Liu, "Control performance analysis and improvement of a modular power converter for three-phase SRM with Y-connected windings and neutral line," *IEEE Trans. Ind. Electron.*, vol. 63, no. 10, pp. 6020–6030, Oct. 2016.

[19] S. Song, Z. Xia, G. Fang, R. Ma, and W. Liu, "Phase current reconstruction and control of 3-phase switched reluctance machine with modular power converter using single dc-link current sensor," *IEEE Trans. Power Electron.*, to be published.

[20] F. Peng, J. Ye, and A. Emadi, "An asymmetric three-level neutral point diode clamped converter for switched reluctance motor drives," *IEEE Trans. Power Electron.*, vol. 32, no. 11, pp. 8618–8631, Nov. 2017.

[21] A. K. Mishra and B. Singh, "Solar photovoltaic array dependent dual output converter based water pumping using switched reluctance motor drive," *IEEE Trans. Ind. Appl.*, vol. 53, no. 6, pp. 5615–5623, Nov./Dec. 2017.

[22] F. Yi and W. Cai, "A quasi-Z-source integrated multiport power converter as switched reluctance motor drives for capacitance reduction and wide-speed-range operation," *IEEE Trans. Power Electron.*, vol. 31, no. 11, pp. 7661–7676, Nov. 2016.

[23] D. H. Lee and J. W. Ahn, "A novel four-level converter and instantaneous switching angle detector for high speed SRM drive," *IEEE Trans. Power Electron.*, vol. 22, no. 5, pp. 2034–2041, Sep. 2007.

[24] J. Liang, D. H. Lee, G. Xu, and J. W. Ahn, "Analysis of passive boost power converter for three-phase SR drive," *IEEE Trans. Ind. Electron.*, vol. 57, no. 9, pp. 2961–2971, Sep. 2010.

[25] A. K. Jain and N. Mohan, "SRM power converter for operation with high demagnetization voltage," *IEEE Trans. Ind. Appl.*, vol. 41, no. 5, pp. 1224–1231, Sep./Oct. 2005.

[26] Y. Hu, C. Gan, W. Cao, C. Li, and S. J. Finney, "Split converter-fed SRM drive for flexible charging in EV/HEV applications," *IEEE Trans. Ind. Electron.*, vol. 62, no. 10, pp. 6085–6095, Oct. 2015.

[27] Y. Hu, X. Song, W. Cao, and B. Ji, "New SR drive with integrated charging capacity for plug-in hybrid electric vehicles (PHEVs)," *IEEE Trans. Ind. Electron.*, vol. 61, no. 10, pp. 5722–5731, Oct. 2014.

[28] Y. Hu, C. Gan, W. Cao, Y. Fang, S. J. Finney, and J. Wu, "Solar PV-powered SRM drive for EVs with flexible energy control functions," *IEEE Trans. Ind. Appl.*, vol. 52, no. 4, pp. 3357–3366, Jul./Aug. 2016.

[29] C. Gan, J. Wu, Y. Hu, S. Yang, W. Cao, and J. M. Guerrero, "New integrated multilevel converter for switched reluctance motor drives in plug-in hybrid electric vehicles with flexible energy conversion," *IEEE Trans. Power Electron.*, vol. 32, no. 5, pp. 3754–3766, May 2017.

[30] C. Gan, N. Jin, Q. Sun, W. Kong, Y. Hu, and L. M. Tolbert, "Multiport bidirectional SRM drives for solar-assisted hybrid electric bus powertrain with flexible driving and self-charging functions," *IEEE Trans. Power Electron.*, to be published.

[31] H. C. Chang and C. M. Liaw, "An integrated driving/charging switched reluctance motor drive using three-phase power module," *IEEE Trans. Ind. Electron.*, vol. 58, no. 5, pp. 1763–1775, May 2011.

[32] C. Y. Yu, J. Tamura, and R. D. Lorenz, "Optimum dc bus voltage analysis and calculation method for inverters/motors with variable dc bus voltage," *IEEE Trans. Ind. Appl.*, vol. 49, no. 6, pp. 2619–2627, Nov./Dec. 2013.

[33] M. Amiri, H. Farzanehfard, and E. Adib, "A nonisolated ultrahigh step down dc–dc converter with low voltage stress," *IEEE Trans. Ind. Electron.*, vol. 65, no. 2, pp. 1273–1280, Feb. 2018.

[34] D. Panda and V. Ramanarayanan, "Reduced acoustic noise variable dc-bus-voltage-based sensorless switched reluctance motor drive for HVAC applications," *IEEE Trans. Ind. Electron.*, vol. 54, no. 4, pp. 2065–2078, Aug. 2007.

[35] H. C. Chang and C. M. Liaw, "On the front-end converter and its control for a battery powered switched-reluctance motor drive," *IEEE Trans. Power Electron.*, vol. 23, no. 4, pp. 2143–2156, Jul. 2008.

[36] K. Hu, P. Yi, and C. Liaw, "An EV SRM drive powered by battery/supercapacitor with G2V and V2H/V2G capabilities," *IEEE Trans. Ind. Electron.*, vol. 62, no. 8, pp. 4714–4727, Aug. 2015.

[37] Y. S. Kumar and G. Poddar, "Control of medium-voltage AC motor drive for wide speed range using modular multilevel converter," *IEEE Trans. Ind. Electron.*, vol. 64, no. 4, pp. 2742–2749, Apr. 2017.

[38] B. Tai, C. Gao, X. Liu, and Z. Chen, "A novel flexible capacitor voltage control strategy for variable-speed drives with modular multilevel converters," *IEEE Trans. Power Electron.*, vol. 32, no. 1, pp. 128–141, Jan. 2017.

[39] M. Quraan, P. Tricoli, S. D'Arco, and L. Piegari, "Efficiency assessment of modular multilevel converters for battery electric vehicles," *IEEE Trans. Power Electron.*, vol. 32, no. 3, pp. 2041–2051, Mar. 2017.

[40] Y. Okazaki *et al.*, "Experimental comparisons between modular multilevel DSCC inverters and TSBC converters for medium-voltage motor drives," *IEEE Trans. Power Electron.*, vol. 32, no. 3, pp. 1805–1817, Mar. 2017.

[41] D. Patil, S. Wang, and L. Gu, "Multilevel converter topologies for high-power high-speed switched reluctance motor: Performance comparison," in *Proc. IEEE Appl. Power Electron. Conf. Expo.*, Long Beach, CA, USA, 2016, pp. 2889–2896.

[42] Q. Chen, D. Xu, L. Xu, J. Wang, Z. Lin, and X. Zhu, "Fault-tolerant operation of a novel dual-channel switched reluctance motor using two 3-phase standard inverters," *IEEE Trans. Appl. Supercond.*, vol. 28, no. 3, pp. 1–5, Apr. 2018.

[43] K. Tungpimolrut, S. Kachapornkul, P. Jitkreeyarn, P. Somsiri, N. Chayopitak, and C. Akira, "Bipolar excitation for double three-phase full bridge converter based three-phase switched reluctance motor drive system," in *Proc. Annu. Conf. IEEE Ind. Electron. Soc.*, Vienna, Austria, 2013, pp. 2626–2631.

[44] H. C. Chang, C. H. Chen, Y. H. Chiang, W. Y. Sean, and C. M. Liaw, "Establishment and control of a three-phase switched reluctance motor drive using intelligent power modules," *IET Elect. Power Appl.*, vol. 4, no. 9, pp. 772–782, Nov. 2010.

[45] S. Chung and O. Trescases, "Hybrid energy storage system with active power-mix control in a dual-chemistry battery pack for light electric vehicles," *IEEE Trans. Transp. Electrific.*, vol. 3, no. 3, pp. 600–617, Sep. 2017.
[46] C. Duan *et al.*, "A solar power assisted battery balancing system for electric vehicles," *IEEE Trans. Transp. Electrific.*, vol. 4, no. 2, pp. 432–443, Jun. 2018.
[47] J. I. Y. Ota, T. Sato, and H. Akagi, "Enhancement of performance, availability, and flexibility of a battery energy storage system based on a modular multilevel cascaded converter (MMCC-SSBC)," *IEEE Trans. Power Electron.*, vol. 31, no. 4, pp. 2791–2799, Apr. 2016.
[48] N. Kawakami *et al.*, "Development of a 500-kW modular multilevel cascade converter for battery energy storage systems," *IEEE Trans. Ind. Appl.*, vol. 50, no. 6, pp. 3902–3910, Nov./Dec. 2014.
[49] Z. Zheng, K. Wang, L. Xu, and Y. Li, "A hybrid cascaded multilevel converter for battery energy management applied in electric vehicles," *IEEE Trans. Power Electron.*, vol. 29, no. 7, pp. 3537–3546, Jul. 2014.
[50] J. Dixon, J. Pereda, C. Castillo, and S. Bosch, "Asymmetrical multilevel inverter for traction drives using only one DC supply," *IEEE Trans. Veh. Technol.*, vol. 59, no. 8, pp. 3736–3743, Oct. 2010.
[51] L. Maharjan, T. Yamagishi, H. Akagi, and J. Asakura, "Fault-tolerant operation of a battery-energy-storage system based on a multilevel cascade PWM converter with star configuration," *IEEE Trans. Power Electron.*, vol. 25, no. 9, pp. 2386–2396, Sep. 2010.
[52] A. Sidhu, A. Izadian, and S. Anwar, "Adaptive nonlinear model-based fault diagnosis of Li-Ion batteries," *IEEE Trans. Ind. Electron.*, vol. 62, no. 2, pp. 1002–1011, Feb. 2015.
[53] A. C. Arenas, S. Onori, and G. Rizzoni, "A control-oriented lithium-ion battery pack model for plug-in hybrid electric vehicle cycle-life studies and system design with consideration of health management," *J. Power Sources*, vol. 279, no. 1, pp. 791–808, Apr. 2015.
[54] Z. Yang, D. Patil, and B. Fahimi, "Online estimation of capacity fade and power fade of lithium-ion batteries based on input–output response technique," *IEEE Trans. Transp. Electrific.*, vol. 4, no. 1, pp. 147–156, Mar. 2018.

Chun Gan (S'14–M'16) received the B.S. and M.S. degrees in power electronics and motor drives from the China University of Mining and Technology, Jiangsu, China, in 2009 and 2012, respectively, and the Ph.D. degree in power electronics and motor drives from Zhejiang University, Hangzhou, China, in 2016.

He is currently a Research Associate with the Department of Electrical Engineering and Computer Science, University of Tennessee, Knoxville, TN, USA. He has authored more than 60 technical papers in leading journals and conference proceedings, including more than 30 IEEE transactions papers. He holds 12 issued/published invention patents. His research interests include high-efficiency power converters, electric vehicles, electrical motor drives, electrical motor design, continuous variable series reactors, high-voltage direct current transmission, and microgrids.

Dr. Gan was the recipient of the 2018 Marie Sklodowska-Curie Actions Seal of Excellence Award from the European Commission, the 2015 Top Ten Excellent Scholar Award, the 2016 Excellent Ph.D. Graduate Award, the 2015 Ph.D. National Scholarship, the 2015 Wang Guosong Scholarship, and the 2014 and 2015 Outstanding Ph.D. Candidate Awards in Zhejiang University.

Qingguo Sun received the B.S. degree in electrical engineering from Qingdao University, Shandong, China, in 2014. He is currently working toward the Ph.D. degree at the College of Electrical Engineering, Zhejiang University, Hangzhou, China.

His research interests include motor design and control in switched reluctance motor, particularly for the optimization of the torque ripple and efficiency of the motor systems.

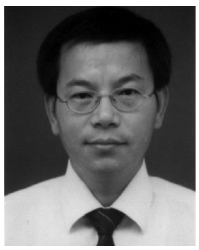

Jianhua Wu received the B.S. degree from the Nanjing University of Aeronautics and Astronautics, Nanjing, China, in 1983, and the M.S. and Ph.D. degrees from the Huazhong University of Science and Technology, Wuhan, China, in 1991 and 1994, respectively, all in electrical engineering.

From 1983 to 1989, he was with Guiyang Electric Company as a Design Engineer. Since 2005, he has been a Professor with the College of Electrical Engineering, Zhejiang University, Hangzhou, China. He developed the motor design software Visual EM-CAD, which is widely used in China. His research interests include electric machine design and drives, including switched reluctance motors, and permanent magnet machines for electric vehicle applications.

Dr. Wu is a member of Electrical Steel of Chinese Society for Metals, the Small-Power Machine Committee of China Electrotechnical Society, and the Standardization Administration of China.

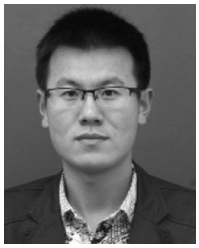

Wubin Kong (M'15) was born in Zhejiang, China, in 1986. He received the B.S. and Ph.D. degrees from Zhejiang University, Hangzhou, China, in 2009 and 2014, respectively.

Since 2015, he has been a Lecturer with the Huazhong University of Science and Technology, Wuhan, China. His research interests include high-power multiphase motor drives and fault-tolerant control motor drive applied in EVs.

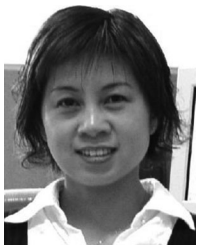

Cenwei Shi received the B.S., M.S., and Ph.D. degrees in electrical engineering from Zhejiang University, Hangzhou, China, in 1991, 1994, and 2001, respectively.

In 1994, she joined Zhejiang University as a Lecturer in electrical engineering. Since 2001, she has been an Associate Professor with the College of Electrical Engineering. In 2003, she spent six months in Germany, as a Visiting Professor with the Institute of Power Electronics and Electrical Drives, Kiel University, Kiel, Germany, working on permanent-magnet motor control. Her main research interests include the design, modeling, simulation, and control of permanent-magnet and reluctance motors.

Yihua Hu (M'13–SM'15) received the B.S. degree in electrical motor drives in 2003, and the Ph.D. degree in power electronics and drives in 2011, both from China University of Mining and Technology, Jiangsu, China.

Between 2011 and 2013, he was with the College of Electrical Engineering, Zhejiang University, Hangzhou, China, as a Postdoctoral Fellow. Between 2013 and 2015, he was a Research Associate with the power electronics and motor drive group, University of Strathclyde, Glasgow, U.K. He is currently a Lecturer with the Department of Electrical Engineering and Electronics, University of Liverpool, Liverpool, U.K. He has authored 55 papers in IEEE transactions journals. His research interests include renewable generation, power electronics converters and control, electric vehicles, more electric ships/aircrafts, smart energy systems, and nondestructive test technology.

Dr. Hu is an Associate Editor for *IET Renewable Power Generation, IET Intelligent Transport Systems,* and *Power Electronics and Drives*.